Structural and Functional Implications of the Instability of the ADP/ATP Transporter Purified from Mitochondria as Revealed by FTIR Spectroscopy

Víctor A. Lórenz-Fonfría,* Joaquim Villaverde,* Véronique Trézéguet,† Guy J.-M. Lauquin,† Gérard Brandolin,‡ and Esteve Padrós*

*Unitat de Biofísica, Departament de Bioquímica i de Biologia Molecular, Facultat de Medicina, Universitat Autònoma de Barcelona, Spain; †Laboratoire de Physiologie Moléculaire et Cellulaire, Institut de Biochimie et Génétique Cellulaires du Centre Nationale de la Recherche Scientifique, Bordeaux, France; and ‡Laboratoire de Biochimie et Biophysique des Systèmes Intégrés, UMR 5092 CEA-CNRS-UJF, Département de Réponse et Dynamique Cellulaires, Commisariat à l'Energie Atomique, Grenoble, France

ABSTRACT The ADP/ATP transporter shows a high instability when solubilized, making it difficult to obtain functional protein with sufficient purity for long-term spectroscopic studies. When solubilized in the detergent dodecyl maltoside the protein is in equilibrium between the so-called CATR and BA conformations and in a few hours it becomes nonfunctional, unable to bind either its inhibitors or its substrates. By Fourier transform infrared spectroscopy, we studied the structural changes involved in this denaturation process. To do so, the carboxyatractyloside-inhibited protein was used as a structural model for the protein in the CATR conformation and its spectrum was compared with that of the unliganded time-inactivated protein. From the difference spectra of the amide I, amide II, and amide A bands combined with dichroism spectra of the carboxyatractyloside-inhibited protein, we concluded that few structural differences exist between both states, affecting as few as 11 amino acids (3.5% of the protein); the structural changes consisted in the disappearance of large loop structure and the appearance of aggregated strands. We hypothesize that some mitochondrial loop (tentatively loop M1) shows a high tendency to aggregate, being responsible for the observed features. The functional consequences of this hypothesis are discussed.

INTRODUCTION

The ADP/ATP transporter is located in the inner mitochondrial membrane, from where it mediates the exchange of cytosolic ADP for ATP generated in the mitochondria. The transporter adopts two structural conformations, which can be detected by its characteristic sensitivity to inhibitors. In the so-called CATR conformation the transporter can be blocked by atractyloside (atr) and carboxyatractyloside (c-atr) acting from the cytosolic side, whereas in the BA conformation the bongkrekic acid (BA) and isobongkrekic acid block the transporter from the matrix side. Both conformations show particular chemical, immunochemical, and enzymatic reactivities, and their interconversions are probably a key feature of the transport process. For further details, see reviews by Brandolin et al. (1993a), Fiore et al. (1998), and Kaplan (1996).

Most of the knowledge about the ADP/ATP transporter has been obtained in experiments performed on mitochondria. In this way, valuable information concerning its function and indirect information about the structural changes involved in the CATR to BA conformation transition has been obtained. However, direct structural information about the ADP/ATP transporter is scarce to date.

Spectroscopic methods can supply part of this information which is currently lacking, provided that the protein is obtained highly pure and in a well-defined conformation. Spectroscopic studies of the ADP/ATP transporter have encountered one major problem: its instability during the purification process (Klingenberg et al., 1995). Since the ADP/ATP transporter is a membrane protein, purification is performed through a solubilized state. In studies performed in very fresh preparations of the solubilized protein, only half of its substrate binding sites are retained (Brandolin et al., 1993b; Krämer and Klingenberg, 1977). Therefore, the solubilized and unliganded ADP/ATP transporter contains a large number of inactive molecules which increase with the time the sample spends solubilized, until reaching full inactivation in a matter of a few hours. The carrier which has lost its capacity to bind ligands in a time-dependent manner will be referred to as *time-inactivated* (Krämer and Klingenberg, 1977). Once reconstituted into liposomes, the transporter remains stable for many hours (Brandolin et al., 1980; Klingenberg et al., 1995). To reduce the time the transporter spends solubilized, the purification procedure can be simplified, so that the reconstituted transporter is obtained only partially purified (50% of contaminating proteins; see Heidkämper et al., 1996; Klingenberg et al., 1995). Obviously, this preparation would not be suitable for spectroscopic analysis. The high instability of the solubilized ADP/ATP transporter entails some questions. Why is it so unstable in the solubilized state? Is the instability related to its function? Which structural changes are responsible for the reduction in the number of binding sites during its isolation?

Submitted November 27, 2002, and accepted for publication March 6, 2003.

Address reprint requests to Esteve Padrós, Unitat de Biofísica, Facultat de Medicina, Universitat Autònoma de Barcelona, 08193 Bellaterra, Barcelona, Spain. Tel.: 34-93-581-1870; Fax: 34-93-581-1907; E-mail: esteve.padros@uab.es.

0006-3495/03/07/255/12 $2.00

In this work, Fourier transform infrared (FTIR) spectroscopy is used, aiming at characterizing the structural changes responsible for the reduction of binding sites during purification of the yeast ADP/ATP transporter from *Saccharomyces cerevisiae* (Anc2pHis; Fiore et al., 2000). FTIR spectra of proteins contain structural information, mainly encoded in band positions of the amide I, but also in the amide II and amide A vibrations (Bandekar, 1992; Goormaghtigh et al., 1994a; Krimm and Bandekar, 1986). Several guides to assign secondary structure from the position of the amide I components have been published; see Arrondo et al. (1993), Goormaghtigh et al. (1994b), and Tamm and Tatulian (1997).

Theoretically, by comparing FTIR spectra of time-inactivated Anc2pHis and fully functional, noninhibited Anc2pHis, we could have some insights into the structural changes responsible for or concomitant with the reduction of the number of binding sites. However, the noninhibited Anc2pHis can have an important proportion of time-inactivated Anc2pHis, growing during the acquisition of infrared spectra. To overcome this problem we considered that the Anc2p when solubilized in dodecyl maltoside (DM) is obtained in equilibrium between the so-called CATR and BA conformations (Roux et al., 1996). Many experimental evidences point to a high structural similarity between the CATR conformation and the c-atr-inhibited state for the beef heart carrier (Brandolin et al., 1993a). Moreover, the c-atr-inhibited state can be considered as a blocked or trapped CATR conformation (Brandolin et al., 1993a; Klingenberg, 1989; Klingenberg et al., 1995). In addition, the high affinity of the c-atr is compatible with a low structural rearrangement of the protein on binding, according to the induced transition fit theory of transport catalysis (Klingenberg, 1989; Klingenberg et al., 1995).

Therefore, in this work, the c-atr-inhibited state is used as a reference state for the noninhibited Anc2p in the CATR conformation, and its structure is compared with that of the time-inactivated unliganded state. FTIR spectra have been obtained for both states (inhibited and time-inactivated) solubilized in the nondenaturing detergent DM (Roux et al., 1996) in solution and dry film, and reconstituted in egg PC/PA phospholipids (dry film).

MATERIALS AND METHODS

Yeast strains and Anc2pHis purification

We used the genetically modified JL1-3-ANC2(His6) *S. cerevisiae* yeast strain, which produced a modified isoform of Anc2p containing the extra sequence GSRSHHHHHH at its C-terminal end (Anc2pHis; Fiore et al., 2000). JL1-3-ANC2(His6) yeast cells were grown as described (Brandolin et al., 1993b). Preparation of yeast mitochondria and purification of Anc2pHis were done as described (Lórenz et al., 2001). All purification steps were carried out at 4°C. Isolated yeast mitochondria were preincubated with carboxyatractyloside (omitted or substituted with atractyloside when the time-inactivated form was purified).

Reconstitution of the Anc2pHis into liposomes

Egg PC/PA (9:1 w/w) presolubilized with DM was added to the purified Anc2pHis at a final lipid-to-protein ratio of 3:1 (w/w) and final DM-to-lipid ratio of 2:1 (w/w). After 1–2 h of incubation at 4°C, Bio-beads were added to a final ratio to DM of 33:1 (w/w). After 6 h of slow stirring at 4°C, the proteoliposomes obtained were centrifuged at 90,000 *g* for 90 min. The pellet was resuspended to the final concentration used in the experiments.

FTIR transmission experiments

Sample preparation

For IR transmission experiments of solubilized samples in solution, the Anc2pHis concentration was 10 mg/ml in DM 9% for the inhibited form, and 15 mg/ml in DM 15% when not inhibited, in Mes 10 mM and NaCl 50 mM (pH 6.8). The sample was placed between two CaF_2 windows using a 6 μm tin spacer. For transmission spectra of dry films of solubilized protein, 0.2–0.1 mg of protein was spread over a CaF_2 window and dried under vacuum.

Spectra acquisition

A total of 1000 scans were co-added in blocks of 40 reference scans and 40 sample scans using a shuttle accessory, with an instrumental resolution of 2 cm^{-1} on a Mattson Polaris FTIR equipped with an MCT detector. The resulting interferogram was apodized with a triangle function, and processed to give absorption spectra at 0.5 cm^{-1} digital resolution. The sample was placed in a circulating water holder connected to a thermostatic bath. An external probe fitted to the sample holder was used to keep the temperature at 25.0°C. The spectrometer compartment was purged with dry air, giving absorption spectra free from water vapor bands.

FTIR attenuated total reflection experiments

Sample preparation

Roughly 40–80 μg of reconstituted Anc2pHis was spread on a 45° trapezoid attenuated total reflection germanium crystal of 50 × 20 × 10 mm. The sample was dried at the atmospheric humidity first, and under a dry nitrogen flow later.

Spectra acquisition

A total of 2000 scans were co-added at an instrumental resolution of 2 cm^{-1} on a Bio-Rad FTS 6000 spectrometer equipped with an MCT detector. The resulting interferogram was apodized with a triangle function, and processed to give absorption spectrum at 0.5 cm^{-1} digital resolution. A cover jacket was placed over the crystal, and connected to a circulating thermostatic bath. The temperature was fixed to 25.0°C, controlled by an external probe fitted to the cover jacket. The spectrometer compartment was purged with dry air. No block averaging was used; under these conditions the presence of residual water vapor peaks in the absorption spectra cannot be fully prevented, so water vapor data were collected and subtracted when needed.

Orientation experiments

Absorption spectra were obtained by using KRS-polarized IR beam parallel (0) or perpendicular (90). The ratio between the total area for a band in both conditions is called the dichroic ratio (R), and is related to the band order parameter of the band transition dipole moment with respect to the crystal normal (p_ϕ; see Eq. 1 in Marsh and Páli, 2001).

When p_ϕ is equal to zero, R is named R_{iso}, which will generally depend on the wavenumber. A dichroism spectrum is obtained as $Abs_{90} - R_{iso}Abs_0$, with the property that only bands having a preferential orientation, different from the magic angle, appears in it. It is thus suited to enhance the resolution of oriented structures of proteins as transmembrane helices. To obtain $R_{iso}(\nu)$, the average values for the electromagnetic fields along the *x*-, *y*-, and *z*-directions should be evaluated. This is a hard task since they depend in a complex way on many parameters, namely: the wavenumber; the angle of the IR beam with the crystal; the refraction index of the crystal; the complex refraction index of the sample; and the thickness of the film over the crystal (Citra and Axelsen, 1996). Under the assumption that the sample is a weak absorber and either the film thickness is much higher than the evanescent wave penetration for all the studied wavenumbers (thick film hypothesis), or it is much lower than the evanescent wave penetration for all the studied wavenumbers (thin film hypothesis), relative expressions can be obtained to evaluate the average electromagnetic fields (Goormaghtigh et al., 1999). If only the weak absorber assumption is made, we can use a semiempirical expression (Eq. 44 in (Goormaghtigh et al., 1999) valid for films outside the thick film and thin film hypothesis. However, we need to evaluate the thickness of the film. To do so we consider the following: Once p_ϕ is obtained, it follows from the properties of the order parameter that for two vibrations from the same molecular structure (e.g., amide I and amide II), the following relation will hold:

$$p_\beta^{\text{Amide I}} = \frac{p_\phi^{\text{Amide I}}}{p_\alpha^{\text{Amide I}}} = \frac{p_\phi^{\text{Amide II}}}{p_\alpha^{\text{Amide II}}} = p_\beta^{\text{Amide II}},$$

where p_α is the order parameter of the transition dipole moment to respect the molecular structure axis and p_β is the order parameter of the molecular structure to respect any other frame of reference with axial symmetry. Since the amide I and amide II bands come from the same molecule their p_β should be equal. For a protein in an α-helix conformation p_α is equal to 0.43 for the amide I and –0.37 for the amide II band (Marsh et al., 2000).

With the information that the order parameter for the transmembrane helices (p_β) obtained from the amide I should be equal to that obtained from the amide II, we can determine the film thickness and the $R_{iso}(\nu)$, and so we can obtain the dichroism spectrum.

Spectral corrections and determination of experimental errors

Buffer subtraction

For transmission experiments in solution, a buffer spectrum was collected and subtracted, to eliminate the contribution of water, detergent, and salts. The subtraction factor was chosen as that leaving a flat baseline between 2000 and 1800 cm^{-1}.

Amino acid side-chain absorption subtraction

A synthetic amino acid side-chain absorption spectrum was constructed (Venyaminov and Kalnin, 1990), taking into account the primary sequence of the Anc2pHis (Le Saux et al., 1996). The subtraction factor was calculated as described (Lórenz et al., 2001).

Phospholipid and DM absorption

The phospholipids used have no significant absorption in the amide I or II, whether between 4000 or 3150 cm^{-1}. DM shows no absorption in the amide I or II, but it does between 3500 and 3100 cm^{-1}. Therefore the amide A, at ~3300 cm^{-1}, is not directly observable for the solubilized protein.

Spectral analysis

Fourier self-deconvolution

It was performed using the program supplied by Spectrum Square Associates, implemented in the GRAMS software (Galactic Industries). The theory of Fourier self-deconvolution (FSD) is well-developed (Lórenz-Fonfría et al., 2002; Moffat and Mantsch, 1992). Our spectra were deconvoluted for a Lorentzian profile of full-width at half-high (FWHH) equal to γ', filtered with a Bessel or a Gaussian function, and a narrowing factor of k (Kauppinen et al., 1981).

Maximum likelihood restoration

It was performed using the program supplied by Spectrum Square Associates, implemented in the GRAMS software (Galactic Industries). Maximum likelihood restoration (MLR) is a nonlinear iterative deconvolution method. Instead of trying to solve directly the deconvolution problem it searches for a solution that, when convoluted by a Lorentzian profile of FWHH equal to γ', matches the experimental spectrum to a certain degree. The method restricts the solution to be positive, but negative values may have a physical meaning if a band if over-deconvoluted or deconvoluted using a wrong profile. To overcome this restriction an offset was added before the analysis and removed after MLR.

Curve-fitting procedures

Curve-fitting was carried out using the program DATAFIT (Spectrum Square Associates) implemented in the GRAMS software. It uses the Levenberg-Marquardt method to find the parameters that yield a minimum χ^2. A maximum of 1000 iterations were used.

The number of bands to fit the amide I were obtained from FSD and MLR spectra. Curve-fitting was performed on deconvoluted spectra. To obtain accurate results on curve-fitting overlapped bands, the form of the component bands should be well characterized. If we assume that amide I component bands are Lorentzian bands, Voigt bands with fixed Gaussian width should be used to fit deconvoluted spectra (Lórenz-Fonfría et al., 2002). If we assume that the amide I component bands have mixed Lorentzian-Gaussian character, Voigt bands with free Gaussian width should be used (Lórenz-Fonfría et al., 2002). Finally, an offset was also included when the fitted spectra contained an absorption-free region.

Calculation and quantification of difference spectra

Difference spectra were obtained by subtracting two absorption spectra with a factor such that the 1700–1610 cm^{-1} interval (amide I) had as much positive as negative area. In transmission experiments, if two identical spectra are subtracted, a zero difference spectrum will be obtained. However, this is not true in attenuated total reflection experiments since the apparent film thickness depends on the actual film thickness and the wavenumber. The consequence is that true difference spectra can only be generally obtained for a short wavenumber interval without artifacts. The quantification of difference spectra was performed in the following way: difference spectra were deconvoluted, and band areas were obtained by integration and/or curve-fitting. In this way the possible area cancellation between positive and negative parts in the difference spectra is minimized. The band areas at the amide I interval were divided by the amide I total area and the same was done for the amide II. This allows us to obtain a percentage of the amino acids involved in the structural changes for both the amide I and amide II.

Fluorescence experiments

Intrinsic fluorescence data was acquired by exciting at 297 nm, using a slit of 4 nm, and collecting at 340 nm with a slit of 16 nm. The sample (1 ml of the

DM-solubilized Anc2pHis at a 0.04 mg/ml) was linearly heated (at 50°C/h) on an AMINCO SLM 8000 fluorimeter (SLM Instruments).

RESULTS

Purity of the samples

The first requirement for this study was to check that the c-atr-inhibited Anc2pHis and the time-inactivated Anc2pHis were obtained pure and in a well-defined state. The SDS-PAGE revealed that the Anc2pHis purity was higher than 95% (not shown). It was more difficult to assure that the protein was obtained in a single conformation. We assumed that the c-atr-inhibited form was almost 100% inhibited, since mitochondria were preincubated with an excess of c-atr, which shows a very high affinity for the Anc2p. An indirect observation of the c-atr binding was obtained from fluorescence experiments. It is known that the intrinsic fluorescence of the Anc2p decreases upon c-atr binding (Brandolin et al., 1993b). When the solubilized c-atr-inhibited Anc2pHis was heated, a fluorescence transition appeared, corresponding to an increase of intrinsic Trp fluorescence (not shown). We assign this fluorescence increase to the release of the c-atr. Moreover, the fluorescence increase was very intense and quite repetitive between different inhibited Anc2pHis purified samples (+99 ± 14%). It is therefore a very sensitive method to detect the presence of c-atr-inhibited Anc2p. When the time-inactivated Anc2pHis (noninhibited or preincubated with the low affinity inhibitor atr) was incubated with ATP (to promote the transition between BA and CATR conformations), c-atr and heated, no fluorescence transition was detected. We concluded that it was totally unable to bind c-atr, and so fully inactivated.

Solubilized Anc2p

Fig. 1 *A* displays the dry film transmittance absorption spectrum of the time-inactivated solubilized Anc2pHis. Previously we have shown that working with dry films does not alter significantly the Anc2pHis structure as revealed by infrared spectroscopy (Lórenz et al., 2001). The amide I appears at 1656.5 cm^{-1} and the amide II at 1545.1 cm^{-1}, which suggests a predominantly helix and/or unordered structure. The spectrum of the inhibited Anc2pHis was presented in a previous work (see Fig. 3 *A* in Lórenz et al., 2001). For the time-inactivated form, the amide I, amide II, and tyrosine appear at a slightly lower wavenumber, suggesting minor structural differences.

Deconvolution and curve-fitting

In Fig 1 *B*, the deconvoluted spectrum of Fig. 1 *A* is presented together with its curve-fitting. In Fig. 1 *C* the deconvoluted spectrum and curve-fitting of the c-atr-inhibited Anc2pHis is displayed for comparative reasons. The most striking differences of Fig. 1 *B* with respect to Fig. 1 *C* are the prominent bands at 1628 cm^{-1} and 1696 cm^{-1} in the noninhibited Anc2pHis, usually observed in aggregation processes induced by temperature (Heimburg and Marsh, 1993). These changes, however, result in only slight differences in the individual band positions, widths and areas, as presented in Table 1. Only three bands change their

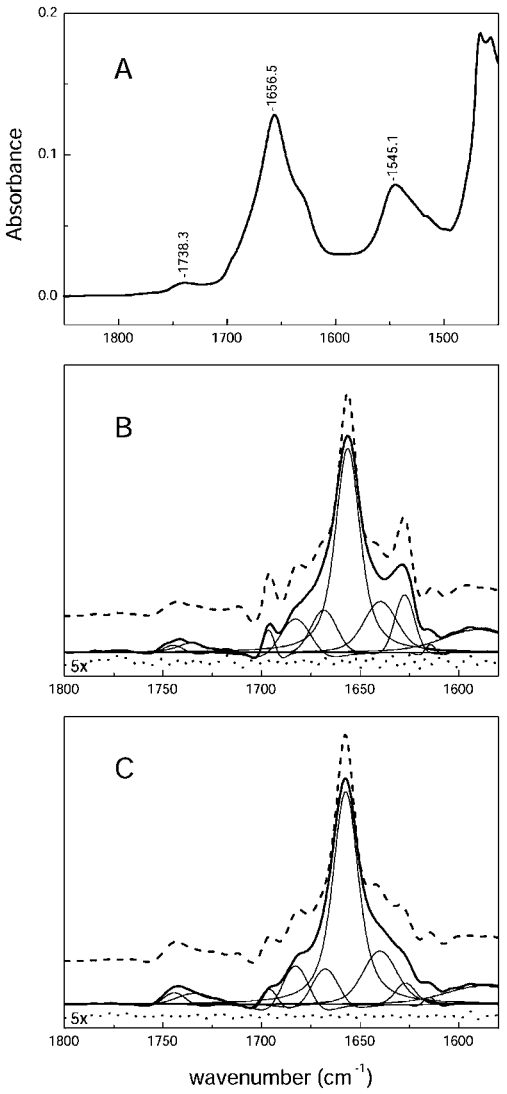

FIGURE 1 (*A*) (——) Transmission absorbance spectrum of a dry film of the DM solubilized time-inactivated Anc2pHis (isolated in the absence of inhibitors), corrected for amino acid side-chain absorption. Spectrum S/N was 2000. (*B*) (- - - - -) MLR ($\gamma' = 18\ cm^{-1}$) of the spectrum in *A*; (——) FSD of the spectrum in (A) ($\gamma' = 18\ cm^{-1}$, $k = 2.0$, and a Gaussian apodization). Curve-fitting was performed with Voigt profiles allowing for optimizing Lorentzian-Gaussian character (as described in Materials and Methods). Fit results are presented in Table 1. (·····) Curve-fitting residual in an enhanced scale and shifted down for a clearer display. (*C*) (- - - - -) MLR ($\gamma' = 18\ cm^{-1}$) of the c-atr-inhibited Anc2pHis. (——) FSD of the c-atr-inhibited Anc2pHis ($\gamma' = 18\ cm^{-1}$, $k = 2.0$, and a Gaussian apodization). Curve-fitting was performed with Voigt profiles allowing for an unknown Lorentzian-Gaussian character. Fit results are presented in Table 1. (·····) Curve-fitting residual in an enhanced scale and shifted down for a clearer display.

TABLE 1

Noninhibited Anc2pHis			Inhibited Anc2pHis				
Position*	FWHH*	Area†	Position*	FWHH*	Area†	ΔArea	Assignments
1696.5 ± 0.1	9 ± 0.5	0.8 ± 0.2	1696.2 ± 0.2	12 ± 0.5	0.7 ± 0.2	+0.1 ± 0.3	β-sheets
1682.8 ± 0.9	22 ± 2	4.9 ± 0.8	1682.9 ± 0.6	19 ± 1	4.5 ± 0.6	+0.4 ± 0.8	turns
1668.5 ± 1.0	24 ± 1	9 ± 0.8	1667.7 ± 1.1	21 ± 1	5.5 ± 0.6	+3.5 ± 1.0	turns
1656.3 ± 0.1	27 ± 0.5	59 ± 1.3	1657.4 ± 0.1	28 ± 0.5	66.3 ± 1.1	−7.3 ± 1.7	α-helix + unordered
1639.7 ± 0.6	31 ± 2	17.4 ± 1.9	1639.9 ± 0.4	31 ± 2	18.8 ± 1.7	−1.4 ± 2.5	β-sheets
1627.4 ± 0.3	20 ± 1	8.9 ± 1.7	1627.0 ± 0.5	22 ± 1	4.1 ± 1.2	+4.8 ± 2.1	β-sheets

Summary of the curve-fit to deconvoluted spectra of noninhibited (Fig. 1 *B*) and carboxyatractyloside-inhibited (Fig. 1 *C*) Anc2pHis in dry film, together with band area differences between both states and band assignments. The errors are standard deviations obtained from Monte Carlo simulations.
*In cm^{-1}.
†Area percentage with respect to all amide I bands.

area significantly: the bands at 1668, 1656, and 1627 cm^{-1}. The secondary structure estimation also presents small changes between the time-inactivated form and the c-atr-inhibited form. If we assume the amide I area to be directly related to the percentage of secondary structure, the structural changes between the inhibited and time-inactivated form are: $\Delta(\alpha\text{-helix} + \text{unordered}) = -7.3 \pm 1.7\%$; $\Delta\beta\text{-sheets} = +3.4 \pm 1.5\%$; and $\Delta\text{turns} = +3.9 \pm 0.8\%$.

Difference spectra

Fig. 2 *A* presents the transmittance absorption spectra for the DM solubilized time-inactivated Anc2pHis and c-atr-inhibited Anc2pHis (scaled to have the same area in the amide I), together with their difference spectra. The difference spectra obtained is rather simple (see Fig. 2 *B*), with only one very well-defined band disappearing in both amide I and amide II regions, and two bands appearing in the amide I and one band in the amide II. After Fourier self-deconvolution of the difference spectrum (see Fig. 3 *A*), the bands appeared more defined but no additional bands were detected. Since the changes in the amide I and amide II regions are of the same type, and the negative and positive bands can be assigned to secondary structures from their position (α-helix + non-ordered and β-sheets respectively), we conclude that the difference spectrum comes from changes in the amino acid peptide bond vibration (and not from amino acid side-chain groups, which would cause different effects in the amide I and the amide II regions). The difference consists in some peptide bonds changing from a secondary structure with amide I and amide II bands at 1662 cm^{-1} and 1548 cm^{-1} respectively, to another secondary structure giving amide I bands at 1627 cm^{-1} and 1697 cm^{-1} and an amide II band at 1522 cm^{-1}. From the area differences obtained from the deconvoluted spectrum in both amide I and amide II, we can conclude that ~3.5% of the amino acids of the protein (≈11 amino acids) are involved in the structural changes. This value is not far from that determined from the curve-fitting of the deconvoluted spectra for the time-inactivated and c-atr-inhibited forms (7%, 22 amino acids), as shown in Table 1. According to the hypothesis that the structure of the c-atr-inhibited form is similar to the *CATR* conformer, the structural changes concomitant with the loss of binding sites are the following: formation of intermolecular antiparallel β-sheets (bands appearing at 1697, 1627, and 1522 cm^{-1}), at the expense of some helix or unordered structure (bands disappearing at 1662, and 1548 cm^{-1}). From Fig. 2 *B* it seems that the number of turns does not significantly vary in the transition to the inactive state. Nevertheless, since turns do not give a single defined vibration, their changes, if there were any, would be poorly defined and more difficult to detect in the difference spectra.

The 1741 cm^{-1} band in the difference spectrum has its origin in the lipid that remains bound to the protein after the last step of the purification. The band appears negative, meaning that the time-inactivated protein retains fewer lipids per protein than the c-atr-inhibited protein. From the area of this band, we conclude that the time-inactivated form retains one third less phospholipid than the inhibited form. This represents a reduction of six phospholipids per Anc2p dimer (Lórenz et al., 2001).

The structural changes presented in Figs. 1 and 2 point to an aggregation process. To rule out the possibility that this aggregation is due to the low concentration of water during film preparation, we obtained the Anc2pHis spectra in solution (for the time-inactivated and c-atr-inhibited forms) together with the difference spectrum. Fig. 2 *C* shows that the level of change in secondary structure (5% of the amino acids involved in the structural change) is similar to that of dry film, but the low S/N and baseline uncertainty reduce the precision of the data obtained from this experiment.

Detailed analysis of the difference spectrum

If our interpretation of the difference spectrum in Fig. 2 *B* is correct, this is an interesting opportunity to gain some insight into the infrared bands corresponding to short segments of only 10 amino acids in a protein composed by more than 300. We used two approaches to obtain this information. The difference spectrum in Fig. 2 *B* was deconvoluted and curve-fitted allowing for an unknown Lorentzian-Gaussian character for the bands (Fig. 3 *A*). In this way, we obtained the

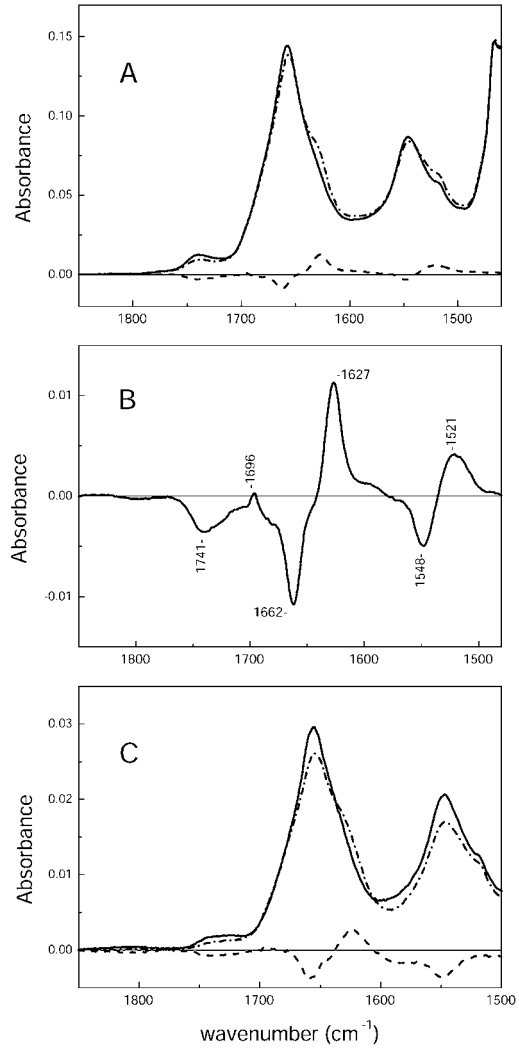

FIGURE 2 (*A*) (——) Dry film of DM solubilized c-atr-inhibited Anc2pHis and (-·-·-) time-inactivated Anc2pHis spectrum scaled to have the same area in the amide I. A DM spectrum was subtracted to compensate differences in the amount of retained detergent. (·····) Difference spectrum between time-inactivated and inhibited forms. (*B*) Difference spectrum in a expanded scale. (*C*) (—) DM solubilized c-atr-inhibited Anc2pHis and (-·-·-) time-inactivated Anc2pHis in solution scaled to have the same area in the amide I. (·····) Difference spectrum between time-inactivated and inhibited forms.

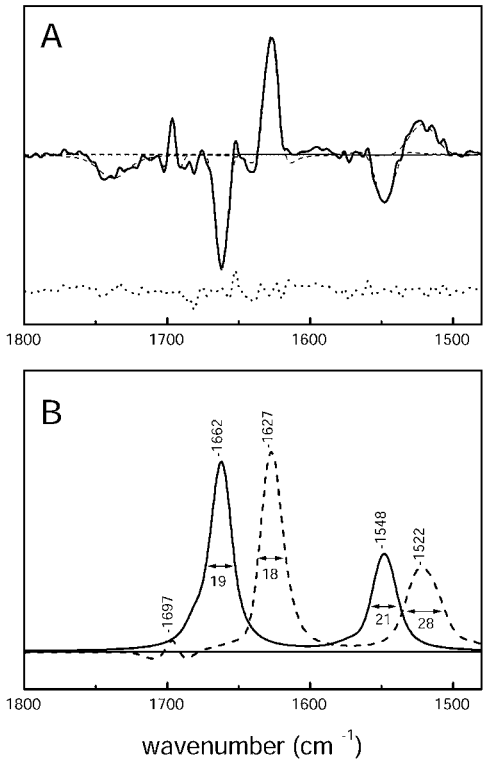

FIGURE 3 (*A*) (——) FSD ($\gamma' = 14$ cm^{-1}, $k = 2$ and Gaussian apodization) of the difference spectrum in Fig. 2 *B*. (- - - - -) Curve-fitting with Voigt bands allowing for Lorentzian-Gaussian character. (·····) Curve-fitting residual shifted down for a clearer display. (*B*) Bands in *A* were extracted and convoluted with a Lorentzian profile of 14 cm^{-1} width. Negative bands in the difference spectrum are shown in continuous line; positive bands are shown in dotted line.

position, area, width, and Lorentzian character percentage for the appearing and disappearing bands. The band parameters obtained are presented in Table 2.

The second approach to study the bands in the difference spectrum also applies FSD but afterwards we do not perform curve-fitting; instead, we extract the resolved bands and reverse the deconvolution process. Fig. 3 *B* shows the amide I and II bands of the lost structures (*continuous line*) and of the new structure (*dotted line*). The advantage of this approach is that we do not need to assume a parametric form for the bands; we only assume that, after FSD, the bands were almost completely resolved.

The results of both analyses can be compared to those of deconvolution of the original spectrum presented in Table 1. We will focus first on the amide I. In the difference spectra, a band disappears at 1662.0 cm^{-1} with a FWHH of 16 cm^{-1}, whereas from Table 1 a band at 1657.4 cm^{-1} with a FWHH of 28 cm^{-1} reduces its area and a band at 1668 cm^{-1} with FWHH of 24 cm^{-1} increases its area. On the other hand, in the difference spectrum a band appears at 1627.3 cm^{-1} with a FWHH of 16 cm^{-1}, whereas from Table 1 a band at 1627.4 cm^{-1} with FWHH of 20 cm^{-1} increases its area. For a protein of this molecular weight the bands obtained by curve-fitting the deconvoluted spectra most likely describe several protein segments whose positions are close enough to remain unresolved. Because frequency proximity usually agrees (with exceptions) with structure similarity for the amide I, the validity of deconvolution plus curve-fitting to predict secondary structure should remain in most cases. However, the use of deconvolution plus curve-fitting to describe subtle structural changes between two states seems less precise than the use of difference spectroscopy combined with curve-fitting or/and deconvolution, since for the first case, the same bands that describe the spectrum also have to describe the changes, which may involve only part of the structure

TABLE 2

Position*	FWHH*	L†	Area	Assignment
1696.4	7	15	+0.2‡	Intermolecular strands
1662.0	16	80	−3.6‡	Large loops
1627.3	16	40	+3.4‡	Intermolecular strands
1547.8	20	40	−3.4§	Large loops
1521.3	28	25	+3.5§	Intermolecular strands

Summary of the curve-fitting to the deconvoluted difference spectrum (noninhibited minus carboxyatractyloside-inhibited Anc2pHis dry film; see Fig. 3 *B*).
*In cm^{-1}.
†Lorentzian intensity percentage.
‡Area percentage with respect to the amide I area.
§Area percentage with respect to the amide II area.

contributing a given component. For the present analysis, the negative band at 1662 cm^{-1} in the difference spectrum requires the variation of two bands in the curve-fitting of deconvoluted spectra (an increase at 1668 and a decrease at 1657 cm^{-1}).

In the case of the amide II region, a band disappears at 1548 cm^{-1} with a FWHH of 20 cm^{-1}, another appearing at 1522 cm^{-1} with a FWHH of 28 cm^{-1}. Amide II bands appear broader and closer than amide I bands.

Reconstitution of Anc2pHis into liposomes and lipid-protein interactions

We first checked the efficiency of the reconstitution by following the lipid/protein ratio obtained in proteoliposomes. From the ratio C=O to amide I of the spectrum of a dry sample, we estimated that both the initial and final lipid/protein ratio in the reconstitution mixtures of the time-inactivated form was 3 (w/w). The efficiency was similar to that of the inhibited protein, where a lipid/protein ratio ~3 was also estimated. Nevertheless, for unknown reasons (probably protein segregation), when mitochondria were not preincubated with atr, the time-inactivated form showed low reconstitution efficiency, giving rise to lipid/protein ratios of 6 or higher.

FTIR analysis of reconstituted Anc2pHis

Fig. 4 *A* shows the absorbance spectra of the time-inactivated reconstituted form (with and without the amino acid side-chain contribution). Fig. 4 *B* displays the deconvoluted spectrum of the side-chain-corrected spectrum, along with that of the inhibited form. Both spectra present differences compared with their solubilized counterparts, suggesting that reconstitution affects the protein structure. Again, the time-inactivated form shows strong bands at 1697 and 1628 cm^{-1} pointing to an aggregation process. The deconvoluted spectra were curve-fitted (not shown). The band differences are similar to those of the solubilized form: the A band at 1659 cm^{-1} decreases its area, whereas bands at 1628, 1670, and 1696 cm^{-1} increase their area. The net result is an increase of turn (+9%) and sheet (+6%) structures and a decrease of helix and unordered structures (−15%).

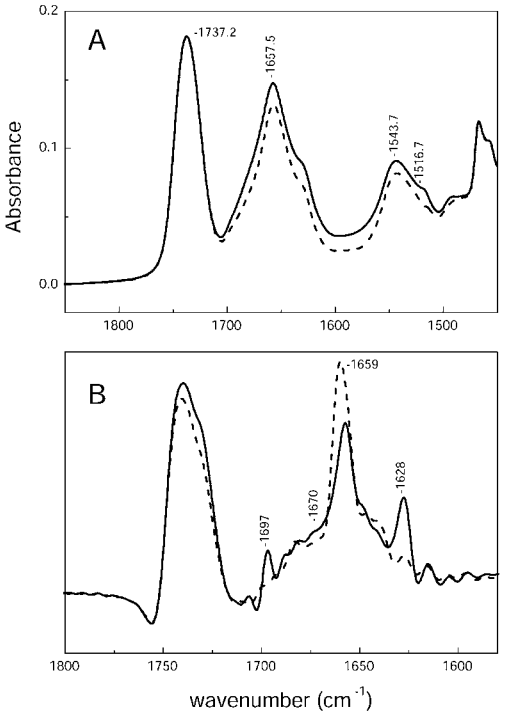

FIGURE 4 (*A*) (——) Attenuated total reflection-FTIR spectrum of a dry film at 25°C of the reconstituted time-inactivated Anc2pHis, corrected for amino acid side-chain absorption. Spectrum S/N was 6500. (*B*) FSD ($\gamma' =$ 18 cm^{-1}, $k = 3$, and Bessel apodization) of (——) the time-inactivated Anc2pHis and (- - - - -) the inhibited Anc2pHis.

Difference spectroscopy between both states (Fig. 5 *A*) gave similar results to those of the solubilized form either in shape or position (compare Fig. 2 *A* with Fig. 5 *A*), with bands appearing at 1696, 1628, and 1524 cm^{-1} and disappearing at 1661 and 1547 cm^{-1}. The difference spectrum for the amide A band gave a band disappearing at 3300 cm^{-1} and a band appearing at 3240 cm^{-1}. The difference spectrum for the amide A was not centered at zero, probably due to slight differences in the amount of retained water in the films. In keeping with amide I and II results, the appearing band can be assigned to β-sheets. Bands at 3300 cm^{-1} have traditionally been assigned to helices (Goormaghtigh et al., 1994a), whereas, to our knowledge, amide A band position for unordered or large loop structures has not been reported.

The amide I difference spectrum was studied further, by FSD followed by curve-fitting and by FSD followed by band isolation and convolution. The results from FSD-band extraction-convolution are presented in Fig. 5 *B* for the amide A, amide I, and amide II bands. The amide I changes accounted for 15% of the amide I area, and so ~7.5% of the protein (25 amino acids) was involved in the structural changes. For rehydrated films (bulk H_2O is deposited over the dry film) amide I difference spectra bands appeared roughly at the same positions (not shown).

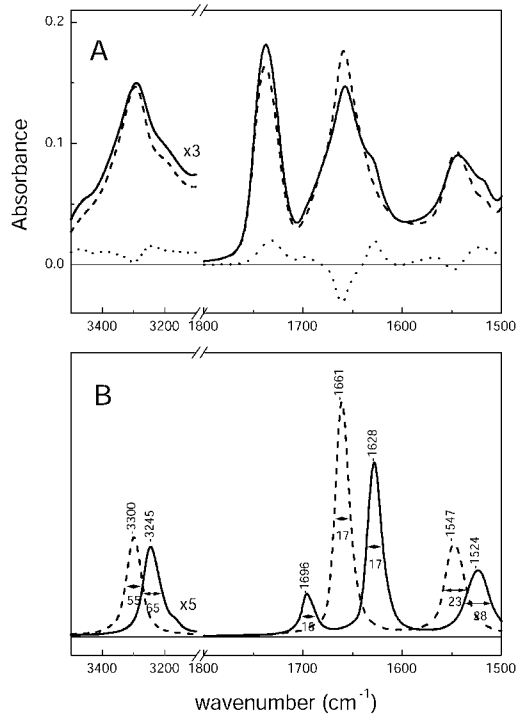

FIGURE 5 (*A*) Samples reconstituted in phospholipid vesicles. (——) Time-inactivated Anc2pHis spectrum and (- - - - -) c-atr-inhibited Anc2pHis spectrum scaled to have the same area at the amide I. (·····) Difference spectrum between the time-inactivated and inhibited reconstituted Anc2pHis. (*B*) Bands in the difference spectrum where resolved by deconvolution, baseline-corrected (for the amide II), extracted, and convoluted back. Band positions and FWHH are displayed. Positive bands in the difference spectrum are shown in continuous line; negative bands are shown in dotted line.

Therefore, it must be concluded that, although different in magnitude from a solubilized to a reconstituted state, the structural changes that prevent the Anc2p from binding its substrates/inhibitors are of the same type, independently of the presence of phospholipid or DM. In other words, once the structural changes that prevent substrate binding happen in the solubilized state, they cannot be reverted by reconstitution into liposomes. In the reconstituted form, the structural differences appear larger, but this is probably because the reconstituted form is obtained later than the solubilized form. In fact, we observed that the intensity of the difference spectrum increases, with time, the sample spent stored.

Effect of SDS

SDS is considered a denaturing detergent promoting the formation of helical segments, preventing the formation of intermolecular interactions and reducing the tertiary interactions (D'Auria et al., 1997; Muga et al., 1993; Torres et al., 1995). Therefore, we analyzed the effect of SDS on both forms of Anc2pHis, in an attempt to distinguish conformational differences caused by the presence or absence of the inhibitor.

When the time-inactivated reconstituted Anc2pHis was solubilized in SDS, a strong structural rearrangement occurred. The aggregation bands disappeared from the IR spectra (Fig. 6), that consisted mainly in an intense and relatively narrow band at 1657 cm^{-1} (70% of the amide I area). However, for the inhibited form the SDS-solubilized protein showed an IR spectrum similar to that of the inhibited form solubilized in DM. It seems that in the absence of inhibitor the protein structure is strongly dependent on the solubilizing detergent. This is coherent with a labile structure for the protein in the absence of inhibitors, that tends either to aggregate (in DM) or to rearrange (in SDS) in accordance with the detergent nature. On the other hand, the structure of the inhibited form is highly insensitive to the detergent nature, probably due to the stabilizing presence of the c-atr.

Orientation experiments

To better perceive the nature of the structure lost in the native to time-inactivated transition, orientation experiments were performed. Based only on band position, the disappearing band at 1661 cm^{-1} cannot univocally be assigned either to transmembrane helices or to unordered structures. Transmembrane helices have a tendency to be ordered to some degree with respect the lipid bilayer normal, hence their amide I and II bands will appear in a dichroism spectrum. Therefore, we compared these bands with those of the difference spectrum. Fig. 7 *A* shows the polarized spectra for the c-atr-inhibited Anc2pHis, together with its dichroism spectrum. The amide bands appeared in the dichroism spectrum at 3296 cm^{-1}, 1658 cm^{-1}, and 1548 cm^{-1}. Even after FSD (see Fig. 7 *B*) the dichroism spectrum appeared rather simple, although two bands were resolved in the amide

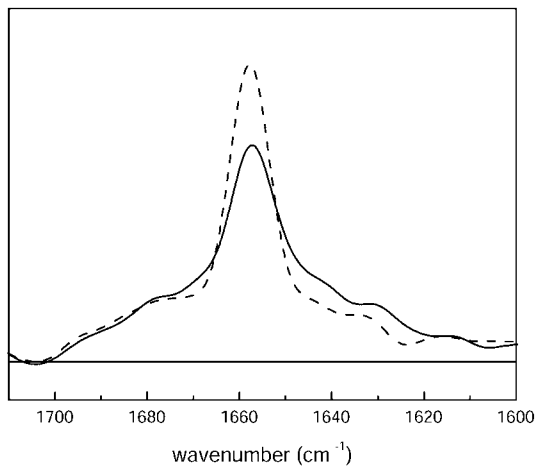

FIGURE 6 Deconvoluted attenuated total reflection-FTIR absorption spectrum (*continuous line*) of the reconstituted c-atr-inhibited Anc2pHis incubated with SDS. Spectrum for the time-inactivated form incubated with SDS (*dashed line*). Deconvolution was performed with $\gamma' = 18$ cm^{-1}, $k = 2.3$, and Bessel filter, and spectra were scaled to the same area between 1700 and 1615 cm^{-1}.

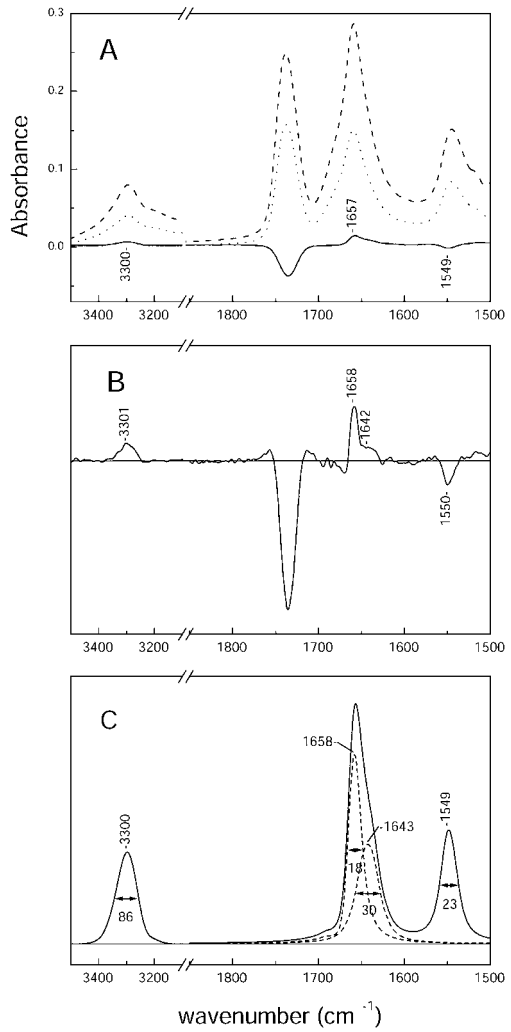

FIGURE 7 (*A*) Attenuated total reflection-FTIR absorption spectrum of the reconstituted Anc2pHis inhibited with c-atr when: (- - - - -) the IR beam was polarized at 90° (Abs_{90}) and (·····) the IR beam was polarized at 0 degrees (Abs_0). (——) Dichroism spectrum obtained as Abs_{90} - $R_{iso} \times Abs_0$ (see Materials and Methods for R_{iso} calculation). The value of R_{iso} at the amide I was 1.81. (*B*) FSD of the dichroism spectrum ($\gamma' = 16\ cm^{-1}$ and $k = 2$ at the amide I and II, and $\gamma' = 50\ cm^{-1}$ and $k = 1.7$ with Gaussian apodization). (*C*) Band obtained after extracting and convoluting the bands in *B*. For the amide I, where the bands are not totally resolved after FSD, the assumptions that the 1658 cm^{-1} deconvoluted band had no absorption down 1643 cm^{-1}, and that the band at 1642 cm^{-1} was symmetrical, were used.

I. In Fig. 7 *C* we present the amide A, I, and II bands for the oriented structures. The band at 1658 cm^{-1} can be assigned to typical transmembrane α-helices, whereas the assignment of the 1643 cm^{-1} is less clear, although it is not important for the present study.

Before we can compare the position of the transmembrane α-helices in the dichroism spectrum with the position of the disappearing band in the difference spectrum we must consider the following: infrared bands coming from α-helices have two close components in the amide I (an intense component and a less intense component at a $\approx$ 4–6 cm^{-1} lower frequency, with different dichroism; see Reisdorf and Krimm, 1995). In absorbance spectra both show positive sign, therefore the α-helix band maximum appears at a slightly lower frequency than the main component. In contrast in a dichroism spectrum of a transmembrane α-helix, the main band has positive intensity, whereas the small band shows negative intensity, the result being a positive band at a higher frequency than the main component. From the position of the band in the dichroism spectrum at 1658 cm^{-1} we can estimate that for the absorbance spectrum the transmembrane α-helix band maximum will be $\sim$1657 cm^{-1}. Therefore, the transmembrane helix seems not to be the structure that disappears in the difference spectrum (at 1661 cm^{-1}), since there exists a 4 cm^{-1} gap in their positions.

DISCUSSION

The Anc2p shows high instability when solubilized, making it difficult to obtain the Anc2p in a native state at sufficient purity for long-term spectroscopic structural studies. We hypothesize that the high tendency of the Anc2p to undergo a structural change that suppresses the binding of its natural substrates/inhibitors could be related to its structural conformation and dynamics in the solubilized state. We aimed at determining the structural changes that prevent Anc2p from binding its substrates/inhibitors, and the cause of this tendency. To this end, Anc2pHis inhibited by c-atr was used as a structural model for Anc2pHis in the *CATR* conformation, and compared with the noninhibited Anc2pHis (that represents unliganded time-inactivated Anc2pHis) by means of FTIR spectroscopy.

Two methods have been used to analyze the structural information contained in the FTIR spectra. First, the protein amide I deconvoluted spectra were curve-fitted and the results compared among the different states. Second, the amide I and amide II (and the amide A in some cases) difference spectra between two states was calculated. Curve-fitting of deconvoluted spectra has the advantage over difference spectroscopy, in that we obtain an estimation of the secondary structure for the studied states. On the other hand, difference spectroscopy has the advantage that spectral features of common structural motives are cancelled out in the subtraction, and differences only appear in the form of positive and negative bands. Therefore, difference spectra seem more appropriate to analyze structural changes between two similar protein states.

When the structure of the noninhibited time-inactivated Anc2pHis was compared to that of the c-atr-inhibited Anc2pHis through the amide A, amide I, and amide II difference spectra, seven well-resolved bands appeared. They were interpreted as arising from formation of intermolecular β-sheets in the time-inactivated state, with bands appearing at 3240, 1697, 1628, and 1524 cm^{-1}. The corresponding disappearing bands at 3300, 1662, and 1547 cm^{-1} come from residues participating in some helix or nonordered structures

in the c-atr-inhibited form. We propose that the structure that disappears in this process corresponds to nonordered structures; more specifically, to large loops. First, it is conceptually difficult to regard a transmembrane helix as a structure prone to forming intermolecular β-sheets without a gross reorganization of the protein structure. Moreover, from data based on the dichroism spectrum, we have shown that the amide I band position of transmembrane helices is shifted by 4 cm^{-1} from the disappearing structure. On the other hand, helices in soluble domains give bands down to 1656 cm^{-1} for the amide I (Goormaghtigh et al., 1994b). Large loops and atypical nonperiodic structures have been assigned at 1655 cm^{-1} in D_2O solutions (Prestrelski et al., 1991; Surewicz and Mantsch, 1988); therefore, in H_2O, they should be expected $\sim$1665–1660 cm^{-1}. The disappearing structure at 1662 cm^{-1} most probably corresponds to this group.

Therefore, FTIR results point to structured large loops (rather than unordered structures) as the feature that is lost on aggregation, although the conclusions we will draw are mainly unaffected by the assignment to large loops or unordered structures. These results were independent of Anc2pHis being in the solubilized state (in DM) or reconstituted (in egg PC/PA), although the number of amino acids involved in the structural changes was higher in the reconstituted form that in the solubilized form. This is probably a time effect, as the reconstituted form requires more time to be obtained than the solubilized form.

From band area quantification, it can be estimated that after a change in the structure of only $\sim$11 amino acids, the binding ability of the protein is lost. This implies that the structure lost in the transition from the *CATR* conformation to time-inactivated Anc2pHis plays a key role in the binding capability. Our hypothesis is that, per Anc2p dimer, at least two (topological) loops facing the matrix side (the so-called M loops; see Fig. 8) form structurally large loops (or unordered structures) which can aggregate to form intermolecular β-sheets, making the protein nonfunctional. This is supported by the evidence that the M loops play an important functional role in the protein, being involved in the substrates/inhibitors binding (especially the M2 loop; see Bogner et al., 1986; Dalbon et al., 1988; and Dianoux et al., 2000), substrates transport (Brandolin et al., 1993a; Majima et al., 1994), and perhaps forming a portion of the translocation pathway (Kaplan, 1996; Klingenberg, 1989). Moreover, the M loops contain many conserved residues (Brandolin et al., 1993a), and some of them have been proven to be essential for the protein function as revealed from site-directed mutagenesis (Müller et al., 1996, 1997). We discarded the involvement of the cytosolic loops in the aggregation process for two reasons: no functional role has been suggested for them, and the C loops are apparently too short to aggregate forming intramolecular β-strands without a more important rearrangement of the protein conformation (Fig. 8).

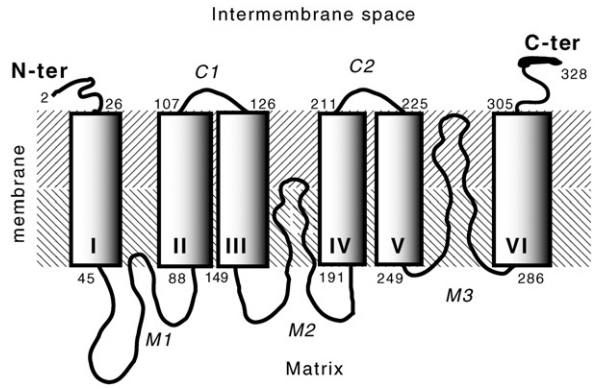

FIGURE 8 Topological model of Anc2p from *S. cerevisiae*. His-tagged Anc2p (328 amino acids) contains six putative transmembrane segments (TMS, I–VI) connected by two cytosolic (C1 and C2) and three matrix (M1, M2, and M3) hydrophilic loops. Arabic numbers denote amino acid positions in the primary structure at the beginning and at the end of each putative TMS. Mature Anc2p starts with an *n*-acetylated N-terminal Ser and is only 317 residues long (Dianoux et al., 2000). Bold line at the C-ter denotes the polyhistidine tag.

In the *CATR* conformation none of the M loops is accessible to membrane impermeable chemical reagents from either the matrix or the cytosolic side, whereas, in the *BA* conformation, the loop M1 and, to a lesser degree, the loop M2 are accessible only from the matrix side (Majima et al., 1994). Enzymatic proteolysis studies showed that the M loops are only accessible from the matrix side in the *BA* conformation, and not from the cytosolic side nor in the *CATR* conformation (Marty et al., 1992). The interconversion between the *BA* and *CATR* conformations (involved in the ADP/ATP transport) seems to consist mainly in the intrusion into the transmembrane region of some of the M loops. Moreover, the loop M1 seems to have an especially high mobility in the *BA* conformation, as revealed by Cys crosslinking (Hashimoto et al., 1999; Majima et al., 1995), which is totally inhibited in the *CATR* conformation. It has been suggested that it acts as a gate for the ATP and ADP binding (Majima et al., 1995). The high mobility of the M1 loops (probably enhanced when solubilized) could allow the interaction between them to form a more energetically stable structure (an antiparallel β-sheet). Although M1 has not been directly related to the binding site, its aggregation could impose such a steric restriction that molecules as bulky as c-atr, BA, ADP, or ATP could not reach the binding site. Moreover, since the *BA* to *CATR* conformation transition involves some reorganization of the M1 loops, its aggregation could impede such a transition.

Although any of the three M loops could show a tendency to aggregation, we tentatively consider the loop M1 as the one that most likely aggregates, given the experimental evidences. We hypothesize that, due to unknown functional reasons, the M1 loop is highly dynamic and this dynamism causes a high instability when solubilizing the Anc2p. The c-atr-inhibited form is thought to be highly stable during

isolation because loop M1 is hidden (not accessible from the matrix side) and in a blocked *CATR* conformation (Hashimoto et al., 1999) that is stable even in the presence of SDS. The BA inhibited form would be partially stable because loop M1 is extended into the matrix but its mobility is probably restricted by the inhibitor presence. Noninhibited Anc2p obtained in the *CATR* conformation probably is able to equilibrate with the *BA* conformation in a relatively short time (hours), even in the absence of the substrates ATP/ADP, from where loops M1 can rapidly aggregate. Finally, when solubilization is performed in the presence of ATP or ADP, the *CATR* and *BA* conformations equilibrate very rapidly, and so the protein could become readily inactivated from the *BA* conformation. This sequence agrees with the stability sequence observed when isolating Anc2p (Klingenberg, 1989).

In conclusion, we hypothesize that the high mobility of a M loop (most probably the M1 loop) allows it to become accessible or inaccessible from the matrix side in the *BA* to *CATR* conformational transition. This high mobility could be responsible for the instability of the Anc2p in the solubilized state. Its aggregation, although affecting very slightly the protein structure, is accompanied by the loss of the protein binding sites. It should be pointed out that this is the first spectroscopic evidence of the importance of the M loops in Anc2p function.

This work was supported by grants Bio4-CT97-2119 from the European Commission to G.L., G.B., and E.P., BMC2000-0121 from the Dirección General de Investigación, Ministerio de Ciencia y Tecnología, and 2001SGR00197 from the Generalitat de Catalunya, and fellowship 1998-FI-00215 from the Generalitat de Catalunya to V.A.L.-F.

REFERENCES

Arrondo, J. L. R., A. Muga, J. Castresana, and F. M. Goñi.1993. Quantitative studies of the structure of proteins in solution by Fourier-transform infrared spectroscopy. *Prog. Biophys. Mol. Biol.* 59:23–56.

Bandekar, J. 1992. Amide modes and protein conformation. *Biochim. Biophys. Acta.* 1120:123–143.

Bogner, W., H. Aquila, and M. Klingenberg. 1986. The transmembrane arrangement of the ADP/ATP carrier as elucidated by the lysine reagent pyridoxal 5-phosphate. *Eur. J. Biochem.* 161:611–620.

Brandolin, G., J. Doussiere, A. Gulik, T. Gulik-Krzywicki, G. J. Lauquin, and P. V. Vignais. 1980. Kinetic, binding and ultrastructural properties of the beef heart adenine nucleotide carrier protein after incorporation into phospholipid vesicles. *Biochim. Biophys. Acta.* 592:592–614.

Brandolin, G., A. Le Saux, V. Trézéguet, G. J. Lauquin, and P. V. Vignais. 1993a. Chemical, immunological, enzymatic, and genetic approaches to studying the arrangement of the peptide chain of the ADP/ATP carrier in the mitochondrial membrane. *J. Bioenerg. Biomembr.* 25:459–472.

Brandolin, G., A. Le Saux, V. Trézéguet, P. V. Vignais, and G. J. Lauquin. 1993b. Biochemical characterisation of the isolated Anc2 adenine nucleotide carrier from *Saccharomyces cerevisiae* mitochondria. *Biochem. Biophys. Res. Commun.* 192:143–150.

Citra, M. J., and P. H. Axelsen. 1996. Determination of molecular order in supported lipid membranes by internal reflection Fourier transform infrared spectroscopy. *Biophys. J.* 71:1796–1805.

Dalbon, P., G. Brandolin, F. Boulay, J. Hoppe, and P. V. Vignais. 1988. Mapping of the nucleotide-binding sites in the ADP/ATP carrier of beef heart mitochondria by photolabeling with 2-azido[α-32P]adenosine diphosphate. *Biochemistry.* 27:5141–5149.

D'Auria, S., R. Barone, M. Rossi, R. Nucci, G. Barone, D. Fessas, E. Bertoli, and F. Tanfani. 1997. Effects of temperature and SDS on the structure of β-glycosidase from the thermophilic archaeon *Sulfolobus solfataricus*. *Biochem. J.* 323:833–840.

Dianoux, A. C., F. Noël, C. Fiore, V. Trézéguet, S. Kieffer, M. Jaquinod, G. J. Lauquin, and G. Brandolin. 2000. Two distinct regions of the yeast mitochondrial ADP/ATP carrier are photolabeled by a new ADP analogue: 2-azido-3′-O-naphthoyl-[β-32P]ADP. Identification of the binding segments by mass spectrometry. *Biochemistry.* 39:11477–11487.

Fiore, C., V. Trézéguet, A. Le Saux, P. Roux, C. Schwimmer, A. C. Dianoux, F. Noël, G. J. Lauquin, G. Brandolin, and P. V. Vignais. 1998. The mitochondrial ADP/ATP carrier: structural, physiological and pathological aspects. *Biochimie.* 80:137–150.

Fiore, C., V. Trézéguet, P. Roux, A. Le Saux, F. Noël, C. Schwimmer, D. Arlot, A. C. Dianoux, G. J. Lauquin, and G. Brandolin. 2000. Purification of histidine-tagged mitochondrial ADP/ATP carrier: influence of the conformational states of the C-terminal region. *Prot. Expr. Purif.* 19:57–65.

Goormaghtigh, E., V. Cabiaux, and J. M. Ruysschaert. 1994a. Determination of soluble and membrane protein structure by Fourier transform infrared spectroscopy. I. Assignments and model compounds. *Subcell. Biochem.* 23:329–362.

Goormaghtigh, E., V. Cabiaux, and J. M. Ruysschaert. 1994b. Determination of soluble and membrane protein structure by Fourier transform infrared spectroscopy. III. Secondary structures. *Subcell. Biochem.* 23:405–450.

Goormaghtigh, E., V. Raussens, and J. M. Ruysschaert. 1999. Attenuated total reflection infrared spectroscopy of proteins and lipids in biological membranes. *Biochim. Biophys. Acta.* 1422:105–185.

Hashimoto, M., E. Majima, S. Goto, Y. Shinohara, and H. Terada. 1999. Fluctuation of the first loop facing the matrix of the mitochondrial ADP/ATP carrier deduced from intermolecular cross-linking of Cys56 residues by bifunctional dimaleimides. *Biochemistry.* 38:1050–1056.

Heidkämper, D., V. Müller, D. R. Nelson, and M. Klingenberg. 1996. Probing the role of positive residues in the ADP/ATP carrier from yeast. The effect of six arginine mutations on transport and the four ATP versus ADP exchange modes. *Biochemistry.* 35:16144–16152.

Heimburg, T., and D. Marsh. 1993. Investigation of secondary and tertiary structural changes of cytochrome c in complexes with anionic lipids using amide hydrogen exchange measurements: an FTIR study. *Biophys. J.* 65:2408–2417.

Kaplan, R. S. 1996. Mitochondrial transport processes. *In* Molecular Biology of Membrane Transport Disorders. S. G. Schultz, T. E. Andreoli, A. M. Brown, D. M. Fambrough, J. F. Hofman, and M. J. Welsh, editors. Plenum Press, New York. pp.277–302.

Kauppinen, J. K., D. J. Moffat, H. H. Mantsch, and D. G. Cameron. 1981. Fourier transforms in the computation of self-deconvoluted and first-order derivative spectra of overlapped band contours. *Anal. Chem.* 53:1454–1457.

Klingenberg, M. 1989. Molecular aspects of the adenine nucleotide carrier from mitochondria. *Arch. Biochem. Biophys.* 270:1–14.

Klingenberg, M., E. Winkler, and S. Huang. 1995. ADP/ATP carrier and uncoupling protein. *Methods Enzymol.* 260:369–389.

Krämer, R., and M. Klingenberg. 1977. Reconstitution of inhibitor binding properties of the isolated adenosine 5′-diphosphate, adenosine 5′-triphosphate carrier-linked binding protein. *Biochemistry.* 16:4954–4961.

Krimm, S., and J. Bandekar. 1986. Vibrational spectroscopy and conformation of peptides, polypeptides, and proteins. *Adv. Protein Chem.* 38:181–364.

Le Saux, A., P. Roux, V. Trézéguet, C. Fiore, C. Schwimmer, A. C. Dianoux, P. V. Vignais, G. Brandolin, and G. J. Lauquin. 1996. Conformational changes of the yeast mitochondrial adenosine diphosphate/adenosine triphosphate carrier studied through its intrinsic fluorescence. 1. Tryptophanyl residues of the carrier can be mutated without impairing protein activity. *Biochemistry.* 35:16116–16124.

Lórenz, V. A., J. Villaverde, V. Trézéguet, G. J. Lauquin, G. Brandolin, and E. Padrós. 2001. The secondary structure of the inhibited mitochondrial ADP/ATP transporter from yeast analyzed by FTIR spectroscopy. *Biochemistry*. 40:8821–8833.

Lórenz-Fonfría, V. A., J. Villaverde, and E. Padrós. 2002. Fourier deconvolution in non self-deconvolving conditions. Effective narrowing, signal-to-noise degradation, and curve fitting. *Appl. Spectrosc.* 56:232–242.

Majima, E., K. Ikawa, M. Takeda, M. Hashimoto, Y. Shinohara, and H. Terada. 1995. Translocation of loops regulates transport activity of mitochondrial ADP/ATP carrier deduced from formation of a specific intermolecular disulfide bridge catalyzed by copper-o-phenanthroline. *J. Biol. Chem.* 270:29548–29554.

Majima, E., Y. Shinohara, N. Yamaguchi, Y. M. Hong, and H. Terada. 1994. Importance of loops of mitochondrial ADP/ATP carrier for its transport activity deduced from reactivities of its cysteine residues with the sulfhydryl reagent eosin-5-maleimide. *Biochemistry*. 33:9530–9536.

Marsh, D., M. Müller, and F. J. Schmitt. 2000. Orientation of the infrared transition moments for an α-helix. *Biophys. J.* 78:2499–2510.

Marsh, D., and T. Páli. 2001. Infrared dichroism from the x-ray structure of bacteriorhodopsin. *Biophys. J.* 80:305–312.

Marty, I., G. Brandolin, J. Gagnon, R. Brasseur, and P. V. Vignais. 1992. Topography of the membrane-bound ADP/ATP carrier assessed by enzymatic proteolysis. *Biochemistry*. 31:4058–4065.

Moffat, D. J., and H. H. Mantsch. 1992. Fourier resolution enhancement of infrared spectra data. *Methods Enzymol.* 210:192–200.

Muga, A., J. L. R. Arrondo, T. Bellon, J. Sancho, and C. Bernabeu. 1993. Structural and functional studies on the interaction of sodium dodecyl sulfate with β-galactosidase. *Arch. Biochem. Biophys.* 300:451–457.

Müller, V., G. Basset, D. R. Nelson, and M. Klingenberg. 1996. Probing the role of positive residues in the ADP/ATP carrier from yeast. The effect of six arginine mutations of oxidative phosphorylation and AAC expression. *Biochemistry*. 35:16132–16143.

Müller, V., D. Heidkämper, D. R. Nelson, and M. Klingenberg. 1997. Mutagenesis of some positive and negative residues occurring in repeat triad residues in the ADP/ATP carrier from yeast. *Biochemistry*. 36: 16008–16018.

Prestrelski, S. J., D. M. Byler, and M. N. Liebman. 1991. Comparison of various molecular forms of bovine trypsin: correlation of infrared spectra with x-ray crystal structures. *Biochemistry*. 30:133–143.

Reisdorf, W. C., Jr., and S. Krimm. 1995. Infrared dichroism of amide I and amide II modes of αI- and αII-helix segments in membrane proteins. *Biophys. J.* 69:271–273.

Roux, P., A. Le Saux, V. Trézéguet, C. Fiore, C. Schwimmer, A. C. Dianoux, P. V. Vignais, G. J. Lauquin, and G. Brandolin. 1996. Conformational changes of the yeast mitochondrial adenosine diphosphate/adenosine triphosphate carrier studied through its intrinsic fluorescence. 2. Assignment of tryptophanyl residues of the carrier to the responses to specific ligands. *Biochemistry*. 35:16125–16131.

Surewicz, W. K., and H. H. Mantsch. 1988. Conformational properties of angiotensin II in aqueous solution and in a lipid environment: a Fourier transform infrared spectroscopic investigation. *J. Am. Chem. Soc.* 110: 4412–4414.

Tamm, L. K., and S. A. Tatulian. 1997. Infrared spectroscopy of proteins and peptides in lipid bilayers. *Q. Rev. Biophys.* 30:365–429.

Torres, J., F. Sepulcre, and E. Padrós. 1995. Conformational changes in bacteriorhodopsin associated with protein-protein interactions: a functional αI-αII helix switch? *Biochemistry*. 34:16320–16326.

Venyaminov, S., and N. N. Kalnin. 1990. Quantitative IR spectrophotometry of peptide compounds in water (H2O) solutions. I. Spectral parameters of amino acid residue absorption bands. *Biopolymers*. 30:1243–1257.